ingegneria sismica
International Journal of Earthquake Engineering
Anno XLIII - Num. 1 - 2026

Exploration of the Molecular Mechanism by Which Calenduloside E Improves Parkinson's Disease by Regulating Mitochondrial Function

Siao Zhang[1], *Kangmei Shao*[1], *Hongwei Guo*[1], *Lilong Ma*[1] *and Jianxiong Li*[1,*]

[1] The Second Clinical Medical College of Lanzhou University, Lanzhou

SUMMARY: *A computational framework oriented to molecular mechanism analysis was constructed to explore the potential chain of action of kalendolide E in improving Parkinson's disease by regulating mitochondrial function. Firstly, based on heterogeneous feature coding and similarity constraint aggregation, mitochondrial dysfunction patterns were identified from 1248 samples, 312 candidate molecules and 8640 high-confidence interaction edges. Combined with drug response, topological proximity, semantic consistency, hierarchical coverage and direction matching, the association features between kalendolide E and mitochondrial regulatory pathways were extracted. Then, a relationship prediction model combining heterogeneous graph propagation, ternary relationship score and ranking loss is constructed to jointly rank the drug-target-pathway-phenotype chain of action. Experimental results show that the AUC of the model reaches 0.948, F1 reaches 0.921, and Hit@20 reaches 85.0%. The results showed that kalendolide E may reduce dopaminergic neuron damage mainly through AMPK-SIRT3 signaling, OPA1-mediated fusion regulation, ATP maintenance and reactive oxygen species control, which provides a computational analysis path for the mechanism of natural active ingredients in Parkinson's disease.*

KEYWORDS: *Molecular relationship prediction; Graph neural network; Mitochondrial function modeling; Mechanism analysis of Parkinson's disease*

1 Introduction

Parkinson's disease (PD) is a nervous system disease characterized by degeneration of dopaminergic neurons in the substantia nigra. The pathological evolution is often accompanied by imbalance of energy metabolism, accumulation of oxidative stress and abnormal dynamic regulation of mitochondria. Mitochondria are not only involved in ATP generation, but also closely related to cell apoptosis, reactive oxygen species scavenging, membrane potential maintenance and neuronal survival. Therefore, molecular mechanism analysis around mitochondrial function has become an important direction in the study of Parkinson's disease. With the development of transcriptome sequencing, protein interaction detection and drug action screening technology, the molecular data related to Parkinson's disease continue to increase. How to use computer methods to extract mechanical-directed structural information from multi-source data has gradually become an important research content in this field.

D 'Sa et al. established a machine learning framework based on the patient-derived stem cell model and realized the prediction of the mechanism subtypes of Parkinson's disease [1]. Payne et al. conducted a multimodal assessment of mitochondrial function in Parkinson's disease and pointed out a strong link between bioenergetic abnormalities and disease

*15991696010@163.com
https://doi.org/10.65102/is2026201 Published: 30 April, 2026

progression [2]. Reddy et al. summarized the application path of artificial intelligence in the early detection and diagnosis of Parkinson's disease [3]. Gupta et al. proposed that artificial intelligence and machine learning methods are pushing Parkinson's disease detection, diagnosis and treatment analysis into a new technical stage [4]. Tabashum et al. systematically combed the development structure and common data types of machine learning models for Parkinson's disease [5]. Altham et al. summarized the multimodal adaptation mode of machine learning in the recognition of cognitive disorders in Parkinson's disease [6]. Hahnel et al. identified progressive subtypes of Parkinson's disease through data-driven multi-cohort analysis [7]. Hossain et al. used speech biomarkers to classify Parkinson's disease patients [8]. Ding et al. proposed a deep learning prediction method based on transcranial ultrasound [9]. Yang et al. proposed a drug-target interaction prediction method MINDG based on ensemble learning algorithm, which combines hybrid deep network, high-order graph attention convolutional network and multi-view adaptive ensemble decision making to improve the accuracy of drug-target relationship recognition [10]. These studies show that artificial intelligence methods have shown strong ability in classification recognition, clinical discrimination and image analysis.

Existing research mainly focuses on disease identification, classification prediction and diagnosis support, and pays less attention to the continuous relationship between drug molecular intervention, mitochondrial function regulation and disease remission mechanism. As a small molecular component with neuroprotective potential, kalendolide E has strong research value in improving oxidative damage, regulating energy metabolism and maintaining mitochondrial homeostasis. Although local targets or individual pathways can be identified by only using traditional experimental pathways, it is difficult to quickly characterize the action chain from multi-layer molecular associations. The introduction of graph structure modeling, relationship prediction and multi-source feature fusion into this kind of mechanism research helps to integrate drug targets, mitochondrial regulatory links and Parkinson's disease-related molecular states into a unified analysis space, thereby improving the systematicity and interpretability of molecular mechanism identification.

Based on this, this paper takes kalendolide E as the research object to construct a computational model for the analysis of the regulatory mechanism of mitochondrial function in Parkinson's disease. In the mitochondrial dysfunction related molecular pattern recognition stage, the disease molecular states are extracted by heterogeneous feature coding and similarity constraint aggregation. In the stage of feature extraction of association between targets and mitochondrial regulatory pathways, molecular response strength, network adjacency and functional semantic distance were combined to characterize the potential regulatory pathways of kalenpolyside E. In the interaction prediction stage, the graph structure propagation and relationship scoring mechanism are used to achieve the joint ranking of key targets, core pathways and functional links. In this way, the information of drug molecules, disease phenotypes and mitochondrial regulation is transformed into learnable association structures, so that the mechanism identification no longer stays in the discrete result comparison, but can complete the continuous expression of the action chain in a unified model.

There are two innovations in this paper. First, the kalenpolyside E intervention information was mapped into the same computational space as the features of mitochondrial dysfunction in PD, which enhanced the structural consistency in the process of molecular mechanism identification. Secondly, the relationship prediction results are used to explain the process of reverse constraint mechanism, so that the correspondence analysis of drug action chain, mitochondrial regulatory chain and disease evolution chain can be completed in a unified model. This study provides a computational and verifiable technical path for the analysis of the effect of kalendolide E on Parkinson's disease, and also provides a more informative analysis method for the study of the drug mechanism of neurodegenerative diseases.

2 Related Research

Research on the molecular mechanism of Parkinson's disease has shifted from single target identification to multi-source biological information fusion analysis. As radiomics, metabolomics, proteomics, single-cell sequencing and graph learning methods continue to enter the research of neurodegenerative diseases, a more complete technical path has gradually formed around the computational modeling of pathological states, molecular markers and drug action chains. Jiang et al. [11] combined radiomics features and deep features for Parkinson's disease prediction in 123I-Ioflupane SPECT, indicating that image representation and deep semantic fusion can improve the ability of disease grading discrimination. de Lope et al. [12] conducted blood metabolomics analysis and found that xanthine metabolism changes had a coordinated relationship with molecular imbalance in Parkinson's disease, which provided a new metabolic layer basis for the study of mitochondrial energy metabolism. Hallqvist et al. [13] established a machine learning recognition model based on the plasma proteome and achieved biomarker prediction at an early stage before the onset of symptoms, showing the prospective value of protein expression combination in the identification of disease progression. Wu et al. [14] combined bioinformatics, machine learning and experimental verification to identify two types of key markers SV2C and DENR, which promoted the integrated expression of candidate gene screening and computational verification.

At the cellular resolution level, Martirosyan et al. [15] used single-cell data to analyze the cell type-specific response of Parkinson's disease, and gave the differential expression trajectories of multiple types of neurons and glial cells. Smajić et al. [16] revealed glial activation and Parkinson-specific neuronal states through single cell sequencing of the human midbrain, which strengthened the structural understanding of disease microenvironment remodeling. Kamath et al. [17] performed single-cell genome mapping of human dopaminergic neurons and identified vulnerable subsets of selective degeneration, providing high-resolution evidence for the localization of disease-sensitive cell types. Kim et al. [18] proposed an artificial intelligence-driven drug relocation strategy and found that Efaveram can regulate α-synuclein propagation, indicating that computational screening is not only suitable for disease identification, but also can enter the link of intervention molecule discovery. The above studies have continuously promoted the research of Parkinson's disease from diagnostic modeling to mechanism modeling, and also provided the basis for integrating small molecule action chains and mitochondrial regulatory chains into a unified analysis framework.

In terms of drug-target relationship modeling, Zhang et al. [19] systematically summarized the application of graph neural network in drug-target interaction prediction, and pointed out that graph representation learning can simultaneously retain molecular structure, network adjacency and biological semantic information. Long et al. [20] further proposed a pre-trained graph neural network framework for biomedical network link prediction, which improved the stability of relationship prediction by integrating multi-source node features. This kind of method has strong adaptability for modeling heterogeneous relationships among small molecules, proteins, pathways and diseases. For a natural active ingredient with potential neuroprotective effects such as kalendolide E, it is difficult to fully describe its continuous molecular links in mitochondrial fusion, oxidative phosphorylation, reactive oxygen species scavenging and neuronal survival regulation if only staying at the level of single experimental pathway comparison. By introducing graph structure propagation, link score and functional constraint into mechanism research, candidate targets, mitochondrial regulatory pathways and Parkinson's disease-related phenotypes can be mapped into learnable association networks, thereby enhancing the structural integrity and result interpretability of mechanism analysis.

From the perspective of technology evolution, the computational focus of Parkinson's disease research has shifted from traditional statistical discrimination to heterogeneous data fusion, graph relationship inference and cross-layer phenotype mapping, and the research object has also expanded from a single diagnostic index to the corresponding structure between pathological links, cell states and drug responses. This change makes the mechanism research closer to computational expression, and also provides methodological support for the subsequent quantitative analysis of the action chain of natural products. The related models are more stable in engineering implementation and result interpretation, and the overall adaptability is higher.

To facilitate the comparison of the above studies in terms of data types and computational paths, Table 1 summarizes the representative works directly related to the task of this paper.

Table 1: Overview of representative work in computational research related to Parkinson's disease

Author	Data Type	Main Method	Inspiration for This Study
Jiang et al. [11]	SPECT imaging	Radiomics combined with deep features	Demonstrates that multi-level feature fusion is suitable for disease state representation.
de Lope et al. [12]	Blood metabolomics	Metabolic profile comparison and molecular association analysis	Provides metabolomic-layer input for modeling mitochondrial metabolic pathways.
Hällqvist et al. [13]	Plasma proteomics	Machine learning identification model	Supports the combined screening of early molecular biomarkers.
Wu et al. [14]	Transcriptomics and validation data	Bioinformatics combined with machine learning	Supports the linkage between key gene screening and cross-validation.
Martirosyan et al. [15], Smajić et al. [16], and Kamath et al. [17]	Single-cell data	Cell subpopulation analysis	Supports the stratified expression of vulnerable cell types and states.
Kim et al. [18]	Drug and pathological propagation data	Artificial intelligence-based drug repositioning	Indicates that computational models can directly support the discovery of intervention molecules.
Zhang et al. [19] and Long et al. [20]	Biomedical networks	Graph neural networks and pre-trained link prediction	Suitable for constructing a heterogeneous network of drug–target–pathway–disease relationships.

In general, the existing research has formed a rich spectrum of methods in image prediction, metabolic marker identification, protein screening, single cell analysis and drug retargeting, but most of the results focus on disease identification, typing discrimination or independent marker screening, and lack a unified model for the mechanism chain of natural small molecules interfering with mitochondrial function and improving Parkinson's disease. Focusing on the association structure between kalendolide E, mitochondrial function and molecular states of Parkinson's disease, this paper adopts a computational route combining molecular pattern recognition, pathway association feature extraction and interaction prediction, so that drug

molecules, disease phenotypes and functional pathways can be jointly analyzed in the same framework.

3 Molecular mechanism of kalendolide E regulating mitochondrial function to improve Parkinson's disease

3.1 Molecular pattern recognition module related to mitochondrial dysfunction in Parkinson's disease

Mitochondrial dysfunction in PD is not a local change caused by a single gene abnormality, but a complex molecular phenotype composed of transcriptional perturbation, protein interaction recombination, decreased membrane potential, reactive oxygen species accumulation, insufficient energy supply and neuronal stress. If the abnormal molecules are judged only by the magnitude of differential expression, it is easy to classify the nodes with similar numerical values but different functional positions into the same class, which weakens the interpretation of the pattern recognition results. Based on this feature, in this paper, the molecular pattern recognition of mitochondrial dysfunction in Parkinson's disease is written as a computational process involving heterogeneous mapping, functional constraints and topological compression, so that the molecular states of cases can be structurally expressed in a unified space. The module receives differential expression data, mitochondrial subcompartment localization annotations, oxidative phosphorylation function labels, reactive oxygen species (ROS) response information, and neuronal damage correlation signals, and writes these information into the same node representation to ensure that the subsequent pattern center updates are based on a unified dimension and common semantics.

In order to more clearly show the composition of the original information entering the pattern recognition module, Table 2 organizes the input data units, computational expression forms and their roles in the module. All kinds of data in the table are not independent of each other, but participate in the molecular state compression in the subsequent joint mapping.

Table 2: Input data composition of the molecular pattern recognition module

Data Type	Main Content	Computational Representation	Module Function
Differential expression data	Expression change values between the case group and the control group	Continuous vector	Describes the magnitude of molecular perturbation
Mitochondrial localization annotation	Labels related to the outer membrane, inner membrane, matrix, and cristae	Categorical embedding	Distinguishes functional spatial locations
Pathway functional labels	Oxidative phosphorylation, fusion and fission, ROS clearance, etc.	Multi-hot encoding	Strengthens functional consistency
Protein–protein interaction relationships	Node adjacency relationships and edge strength	Adjacency matrix	Forms the basis for structural propagation
Neuronal damage signals	Vulnerability state and apoptosis-associated scores	Continuous scalar	Connects to the disease phenotype layer

In order to transform the heterogeneous molecular input into a unified learnable

representation and weaken the interference of extreme values on the central position at the beginning stage of pattern recognition, we jointly map the expression perturbation, functional score and network propagation contribution. The mapping is not an ordinary linear superposition, but a node representation with functional direction is formed under a unified scale, as shown in equation (1).

$$z_i=\alpha\cdot\frac{e_i-\min(E)}{\max(E)-\min(E)}+\beta\cdot g_i+\gamma\cdot\frac{c_i}{1+\deg(i)} \tag{1}$$

Here, z_i represents the joint pattern strength of the i molecule. e_i represents the expression perturbation value between the case group and the control group. E denotes the expression set of all candidate molecules; g_i represents the functional score formed by the combination of mitochondrial localization, oxidative phosphorylation engagement, and reactive oxygen species response tags; c_i represents the propagation contribution of nodes in the local interaction network. $\deg(i)$ represents the degree of node connectivity. α, β, γ represent the fusion weights of expression layer, function layer, and structure layer, respectively. The effect of this formulation is to compress molecular information that is otherwise separated from each other into a unified representation, enabling the pattern center calculation to be built on the same scale while preserving the functional orientation and network location of each molecule.

Fig. 1 illustrates the overall processing path of the recognition module in this section. The leftmost part of the figure is the original input layer, which contains the differential expression matrix, mitochondrial localization annotation, functional labels and interaction network. The first layer in the middle is the heterogeneous mapping layer, in which dimension unification and joint coding are completed. The second layer is the consistency correction layer, which imposes function label constraints and local topology correction on the node representation. On the right is the pattern output layer, which gives the core molecular pattern clusters under different mitochondrial damage states. The key point highlighted in this figure is not graphical complexity, but rather how molecular states progressively converge from discrete inputs to interpretable patterns.

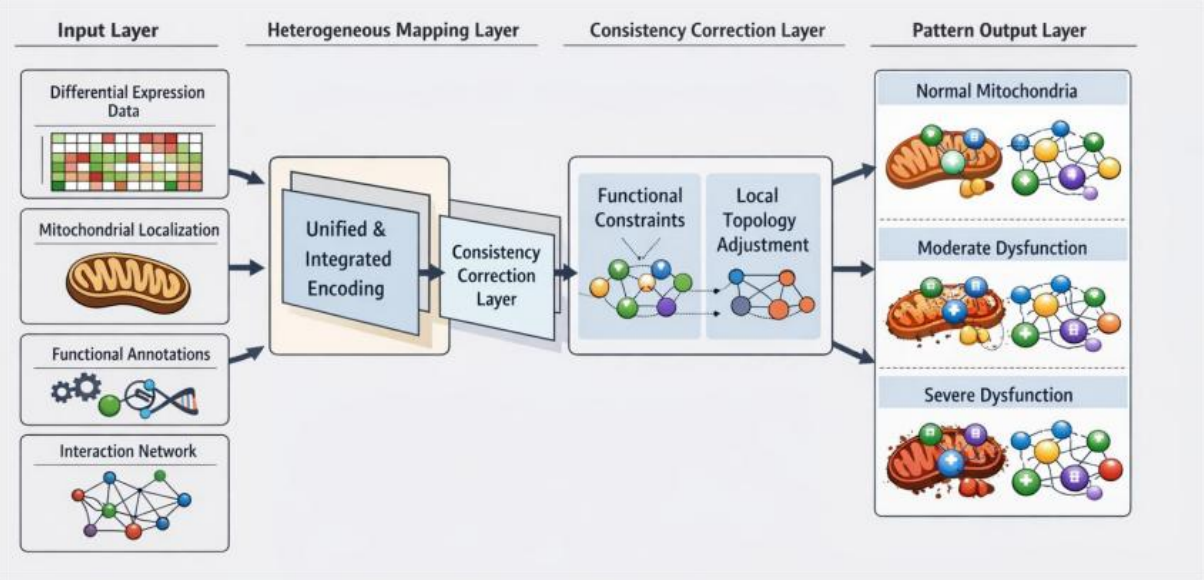

Figure 1: Flowchart for molecular pattern recognition of mitochondrial dysfunction in Parkinson's disease

The joint mapping alone is still not enough to form molecular patterns with stable boundaries, so we continue to introduce the density-condensation collaborative score to compare the reliability of different candidate pattern centers. This score considers both the clustering degree of nodes to the center and the average difference between molecules in the cluster, which can avoid the offset caused by the fuzzy cluster boundary, as shown in equation (2).

$$S_k=\frac{\sum_{i\in\Omega_k}\exp\left(-\|z_i-\mu_k\|_2^2\right)}{1+\sum_{i\in\Omega_k}\sum_{j\in\Omega_k}\frac{\|z_i-z_j\|_1}{|\Omega_k|^2}} \tag{2}$$

where, S_k represents the central reliability of the k pattern cluster. Let Ω_k denote the set of nodes belonging to the pattern; μ_k represents the center of the pattern; $\|\cdot\|_2$ denotes the Euclidean norm; $\|\cdot\|_1$ denotes the Manhattan norm. The smaller the distance between the molecule and the center and the lower the average difference within the cluster, the larger S_k means the more stable the center of the pattern. The significance of this formula is not only to evaluate the quality of clustering, but also to establish a structural basis with functional boundaries and density constraints for disease molecular states, so that the pattern recognition results have higher mechanism interpretation ability.

After pattern clusters are formed, in order to further compress the output structure of this section, Table 3 summarizes the four categories of core mitochondrial dysfunction patterns generated by the recognition module.

Table 3: Output structures for molecular patterns of mitochondrial dysfunction

Pattern Category	Main Molecular Features	Corresponding Mitochondrial State	Structural Implication
Respiratory chain inhibition pattern	Overall downregulation of complex-related molecules	Reduced ATP production capacity	Indicates restricted energy supply
Fusion–fission imbalance pattern	Shifted expression of dynamic regulatory molecules	Weakened morphological homeostasis	Indicates disrupted structural renewal
Oxidative stress enhancement pattern	Sustained activation of ROS-responsive molecules	Accumulated oxidative damage	Indicates an imbalance in clearance capacity
Apoptosis-coupled pattern	Synchronous changes in apoptosis-related molecules	Reduced neuronal survival state	Indicates that damage has extended to the phenotypic layer

Fig. 2 illustrates the internal structure of pattern center update and cluster boundary convergence. The middle and lower layers of the figure show node-level joint vector input, the middle layer shows similarity comparison, center iteration and boundary adjustment, and the upper layer shows the final pattern cluster output and its correspondence with functional labels.

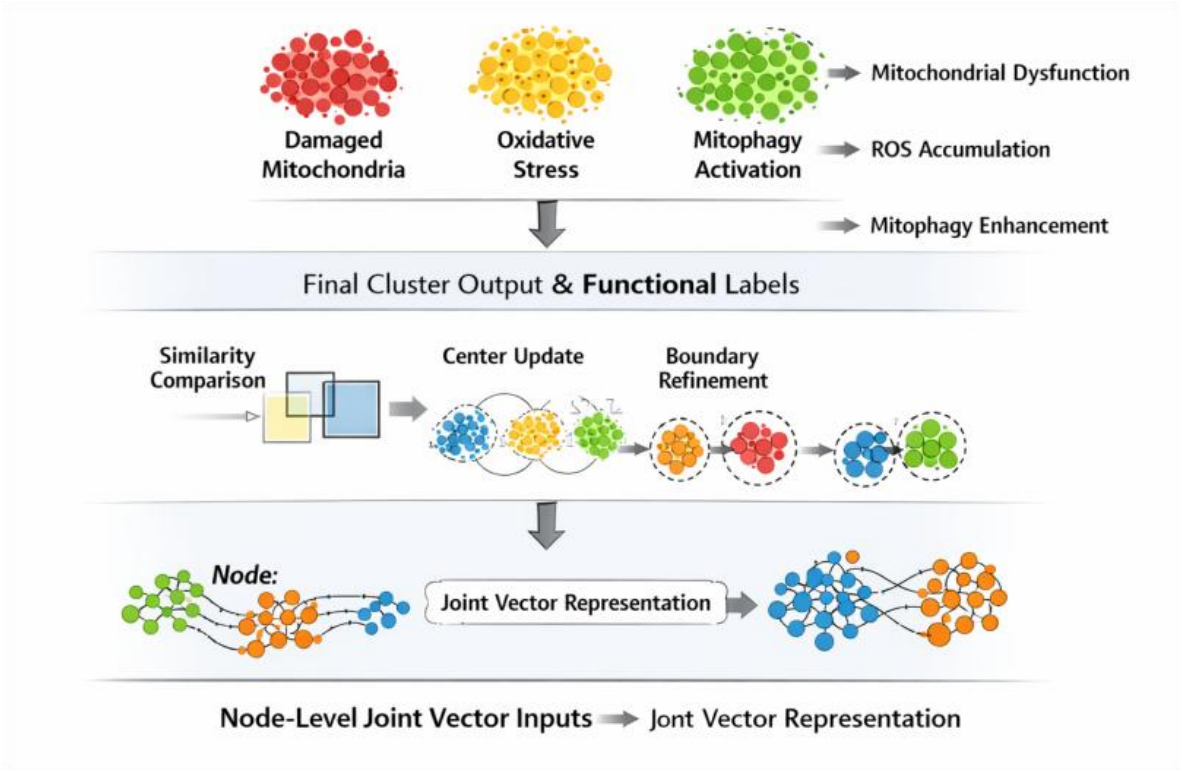

Figure 2: Center update and output structure diagram of mitochondrial damage molecular patterns

After processing in this section, Parkinsonian mitochondrial dysfunction related molecules have been transformed from a loose set of candidate nodes to a stable pattern cluster with center, boundary and functional direction. The pattern expression formed in this way can accurately reflect the state of mitochondrial damage such as respiratory chain inhibition, morphological regulation imbalance, oxidative stress accumulation and enhanced apoptosis coupling, and also upgrade the molecular background of disease from discrete data level to structured pattern level.

3.2 Feature extraction of association between kalendolide E targets and mitochondrial regulatory pathways

In order to ensure that the candidate target response values can remain comparable in subsequent calculations, this paper first compresses the initial value of the direct interaction between kalendolide E and the target. This initial value not only considers molecular docking or binding matching distance, but also incorporates expression response and mitochondrial function annotation information before and after intervention to avoid a single score dominating subsequent results. In other words, the initial response of the target is not the direct transfer of a single experimental quantity, but the fusion expression of multiple evidences under a unified scale. The response values thus obtained can be directly involved in network propagation and pathway mapping, making the drug action structurally oriented from the beginning.

In order to express the direct response of kalendolipid E to candidate targets as a continuous and propagable score, this paper will jointly compress the distance, expression response and functional confidence. The design purpose of this formula is to weaken the over-strong traction of high scores of single items on the overall ranking while preserving the differences in drug effects, as shown in Formula (3).

$$r_i=\lambda_1\cdot\sigma(-d_i)+\lambda_2\cdot\tanh(\Delta_i)+\lambda_3\cdot q_i \tag{3}$$

Here, r_i represents the initial response of kalendolipid E to the i candidate target. d_i represents the molecular binding or matching distance; Δ_i represents the poor expression response before and after drug intervention; q_i indicates the confidence of the target in mitochondrial function annotation; $\sigma(\cdot)$ is the Sigmoid function. $\tanh(\cdot)$ denotes the hyperbolic tangent function; λ_1 to λ_3 represent the fusion weights of the three types of information. The significance of this formula is to transform the multi-source drug response evidence into a single propagable signal, so that the subsequent pathway feature extraction is established on a unified basis.

After the initial target response is generated, this paper further measures the topological proximity between the target and the mitochondrial regulatory pathway. The reason for introducing this quantity is that a high drug response value does not mean that the target must be located on the main pathway of the mechanism. Only when the target maintains a short and stable connection with the critical pathway in the network position, the subsequent relationship interpretation has structural support, as shown in Equation (4).

$$u_{i,p}=\frac{1}{|\Pi_{i,p}|}\sum_{\pi\in\Pi_{i,p}}\exp^{(-\eta\cdot L(\pi)}) \tag{4}$$

Here, $u_{i,p}$ represents the topological proximity between candidate target i and pathway p. Let $\Pi_{i,p}$ denote the set of all feasible paths from the target to the set of pathway nodes. $L(\pi)$ is the length of the path π. Let η denote the length attenuation coefficient. The larger this quantity is, the more likely the target is to affect the corresponding pathway through the shorter path. The function of the formula is to transform the geometric relationship of the network into a continuous index, and provide a structural basis for the position judgment of the mechanism chain.

Topological proximity alone is still insufficient to determine whether drug effects and pathway functions truly match, so we continue to introduce functional semantic consistency to measure the fit between target annotations and pathway topics. In this way, some nodes whose functional meaning deviates from the mitochondrial regulatory core despite their short distance can be avoided from getting too high weight, as shown in equation (5).

$$v_{i,p}=\frac{a_i\cdot b_p}{\|a_i\|_2\|b_p\|_2+\varepsilon} \tag{5}$$

Here, a_i represents the functional semantic vector of target i; b_p represents the topic semantic vector of pathway p; Let ε denote the minimal constant that prevents the denominator from being zero. The significance of this formula is to convert the word-level functional annotation into similarity in continuous space, so that topics such as "mitochondrial fusion", "oxidative phosphorylation" and "ROS scavenging" can be aligned with the target in a unified way.

Considering that the pathway is not a flat structure, but has hierarchical differentiation such as upstream regulation, midstream transmission and downstream execution, we further introduce hierarchical coverage to measure whether the effects of kalenpolyside E can penetrate multiple levels within the pathway, rather than just hitting local nodes. The higher the quantity, the more continuous modulating ability of drug action in the pathway, as shown in equation (6).

$$c_p=\frac{\sum_{l=1}^{H} I(n_l>0)\cdot\omega_l}{\sum_{l=1}^{H}\omega_l} \tag{6}$$

Here, c_p denotes the hierarchical coverage of path p; H represents the total number of pathway levels. n_l represents the number of nodes hit by carenoglycoside E-related targets in layer l; $I(\cdot)$ denotes the indicator function; Let ω_l denote the weight of this layer in the pathway structure. The function of this formulation is to avoid the model from drawing too strong conclusions based only on individual high response nodes, thus improving the continuity of the expression of the mechanism chain.

After completing the calculation of initial response, topological proximity, semantic consistency and hierarchical coverage, it is also necessary to determine whether the regulation direction of kalenoglycoside E forms a reverse correspondence with the state of mitochondrial damage in Parkinson's disease. To this end, the direction matching term is introduced in this paper, as shown in Equation (7).

$$m_{i,p}=\frac{\sum_{t=1}^{T}\omega_t\ \delta_{i,t}\ (-\rho_{p,t})}{\sqrt{\sum_{t=1}^{T}\omega_t\ \delta_{i,t}^2}\sqrt{\sum_{t=1}^{T}\omega_t\ \rho_{p,t}^2}+\varepsilon} \tag{7}$$

Here, $m_{i,p}$ represents the directional matching strength between target i and pathway p. Let $\delta_{i,t}$ denote the regulation value of the drug on the t state channel. Let $\rho_{p,t}$ denote the perturbation value in the t channel of the pathway in the disease state. Let ω_t denote the channel weight; T represents the total number of channels; Let ε denote the minimal constant. The larger $m_{i,p}$ is, the closer the drug action is to the reverse regulation of the disease abnormality. This formula preserves both the direction information and the amplitude of action, so it is more suitable to describe the continuous changes in the recovery of mitochondrial function than only comparing the positive and negative signs.

When the initial response, topological proximity, semantic consistency, hierarchical coverage and direction consistency are all calculated, this paper continues to compress these five types of evidence into unified association features that can be directly entered into the relationship prediction model, as shown in Equation (8).

$$\phi_{i,p}=\theta_1 r_i+\theta_2 u_{i,p}+\theta_3 v_{i,p}+\theta_4 c_p+\theta_5 m_{i,p} \tag{8}$$

Here, $\phi_{i,p}$ represents the comprehensive association characteristics between the candidate target i of kalendolide E and the mitochondrial regulatory pathway p. θ_1 to θ_5 represent the fusion coefficients of the five types of evidence. The function of this formula is not only to complete the feature splicing, but to write the local response, network position, functional meaning and regulation direction into the same vector, so that the structural representation of the drug action chain is more complete.

Fig. 3 shows the complete path of association feature extraction in this section. In the figure, the leftmost part is the drug response initialization layer, the middle part is the topological proximity calculation, semantic consistency matching, hierarchical coverage statistics and direction consistency correction, and the rightmost part outputs the comprehensive pathway association features. Instead of parallel modules, each layer in the figure is a continuous calculation chain, which aims to compress the candidate roles of carenoglycoside E into a structured pathway association vector.

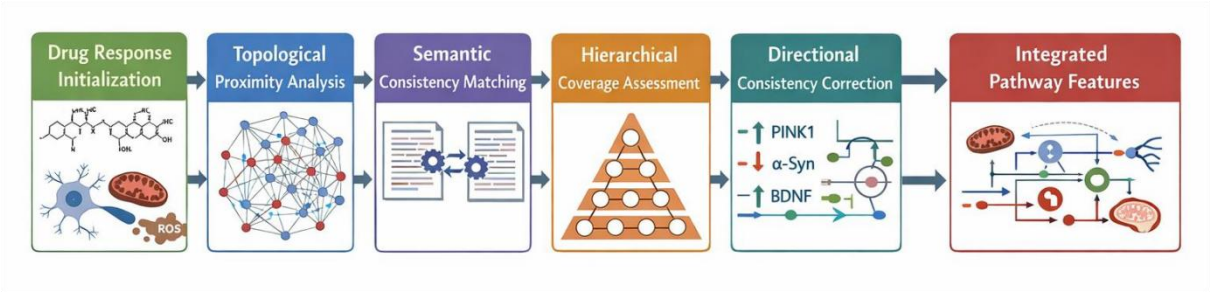

Figure 3: Framework diagram for feature extraction of association between kalendolide E targets and mitochondrial regulatory pathways

After the treatment in this section, the effect of kalendolipid E is no longer manifested as a number of candidate target response values separated from each other, but forms a pathway association feature with location, semantic, hierarchical and directional information. Such feature expression is closer to the true molecular mechanism than single target ranking, because it retains both the strength of drug action and the structural constraints inside the mitochondrial regulatory chain.

3.3 Construction of carenpolyside E interaction prediction model for molecular mechanism analysis

After the molecular pattern recognition of disease and the extraction of drug-pathway association features, this paper further constructs a prediction model of carenoglycoside E interaction for molecular mechanism analysis. The goal of the model is not to give a pure binary classification output, but to jointly score and rank the continuous interaction chain of "drug-target-pathway-phenotype", so as to screen out the relationship combinations that are most likely to form the main pathway of the mechanism. To achieve this goal, kalenpolyside E, candidate targets, mitochondrial regulatory pathways and PD phenotypic states are written as different types of nodes in a heterogeneous graph, while binding relationships, functional participation relationships, transmission direction relationships and disease reversal relationships are encoded as edge attributes.

In order to make different types of nodes still retain their own semantic characteristics when entering the same relational space, this paper first performs heterogeneous projection on drug nodes, target nodes, pathway nodes and phenotype nodes. The projection phase does not use a single mapping matrix, but sets the transformation parameters according to the node type, and then completes the alignment in the public space, as shown in Equation (9).

$$p_i = \tanh\left(x_i M_{\tau(i)} + b_{\tau(i)}\right) \tag{9}$$

where p_i denotes the initial embedding of node i; x_i represents the original input features; Let $\tau(i)$ denote the node type. $M_{\tau(i)}$ and $b_{\tau(i)}$ denote the projection matrix and bias term of the node of this type, respectively. The function of this formula is to ensure that the intra-genre compression and inter-genre alignment of drug structure features, target molecular features, pathway semantic features and phenotypic state features are completed before entering the unified relation space, so that the subsequent propagation maintains a high genre resolution.

After node embedding is generated, the model needs to recharacterize the importance of edge relationships. Since different edges not only represent different biological connections, but also bear different mechanism strengths, in this paper, the edge weight is written as the joint normalization result of the comprehensive association strength, direction consistency and

historical evidence confidence, as shown in Equation (10).

$$w_{ij}=\frac{\exp\left(\kappa_1 s_{ij}+\kappa_2 d_{ij}+\kappa_3 h_{ij}\right)}{\sum_{j'\in R(i)}\exp\left(\kappa_1 s_{ij'}+\kappa_2 d_{ij'}+\kappa_3 h_{ij'}\right)} \tag{10}$$

Here, w_{ij} denotes the normalized edge weight from node i to node j. s_{ij} denotes the comprehensive association strength; d_{ij} denotes directional consistency; h_{ij} denotes the confidence of historical evidence; $R(i)$ denotes the set of neighbors connected to node i; κ_1 to κ_3 represent the weight coefficients of the three types of evidence. The function of this formula is to compress the multi-source edge attributes into a unified propagation weight, so that the relationships with real mechanism significance can obtain higher retention in the network.

When the edge weight update is completed, this paper proceeds with multi-step propagation of node states. The propagation process not only retains the existing state of the current node, but also absorbs the information of the adjacent nodes after edge weight adjustment, so as to form the relationship expression with path memory, as shown in Formula (11).

$$q_i^{(t+1)}=\rho q_i^{(t)}+(1-\rho)\sum_{j\in R(i)} w_{ij}\, p_j \tag{11}$$

Here, $q_i^{(t)}$ represents the state vector of node i after the t round of propagation. Let ρ denote the historical state retention coefficient. The function of this formulation is to enable continuous propagation of drug effects along targets and pathways, while avoiding over-smoothing of states caused by deep propagation, thus preserving local differences and chain structure information.

In order to extract drug-target-pathway relationships with mechanism pointing from node states after propagation, this paper uses ternary coupling score to judge the degree of synergy of different relationship combinations. This score is no longer satisfied with the local connection between two nodes, but simultaneously requires that the three drugs, targets and pathways form a stable coupling in a unified space, as shown in Equation (12).

$$y_{d,t,p}=\frac{(q_d\odot q_t)\cdot q_p}{\|q_d\|_2\|q_t\|_2\|q_p\|_2+\epsilon} \tag{12}$$

Here, $y_{d,t,p}$ represent the ternary relationship score composed of drug d, target t and pathway p. $\odot$ indicates Hadamard product; Let ϵ denote the minimal stable term. The significance of this formula is to extend the drug action chain from binary relationship to ternary synergistic relationship, so as to be closer to the real molecular mechanism expression.

The ternary relationship score alone is still insufficient to indicate whether the chain of action truly corresponds to disease improvement, so this paper continues to include the degree of phenotypic reversal in the overall score. The purpose of this is to make the high-score relationship not only show structural coupling, but also form a reverse regulation of the Parkinson's disease mitochondrial damage phenotype, as shown in equation (13).

$$\psi_{d,t,p}=\mu_1 y_{d,t,p}+\mu_2\xi_p+\mu_3\zeta_t \tag{13}$$

Here, $\psi_{d,t,p}$ represents the comprehensive mechanism relationship score; Let ξ_p denote

the phenotypic contribution of pathway p to the recovery of mitochondrial function. Let ζ_t denote the degree of empirical support of target t for disease reversal; μ_1 to μ_3 represent the fusion coefficients. The effect of this formula is that the relationship prediction results directly correspond to the disease status improvement, so that the model output has a stronger mechanistic explanation ability.

In order to make the training phase pay more attention to the distinction between the true mechanism relationship and the high confidence negative samples, this paper adopts the ranking loss to update the parameters. Different from the ordinary classification loss, the ranking loss pays more attention to the stability of the main path in the front position, so it is more suitable for the mechanism relationship screening task in this study, as shown in Equation (14).

$$L= \sum_{(a,b)\in P} \ln\left(1+\exp\left(-(\psi_a-\psi_b)\right)\right) +\lambda\|\Theta\|_2^2 \tag{14}$$

where P represents the set of positive and negative relation pairs; ψ_a and ψ_b represent the comprehensive mechanism relationship scores of positive and negative samples, respectively. Θ represents all parameters to be learned; Let λ denote the regularization coefficient. The effect of this formula is to push the chain of true mechanisms to the top of the ranking continuously and limit the excessive inflation of model parameters, thereby improving the stability of the training phase.

After the training is completed, the normalized probability output formula is used to generate the final relationship probability of different action chains of kalenpolyside E, and the main path screening of the mechanism is completed according to this probability, as shown in Formula (15).

$$P_{d,t,p}=\frac{\exp\left(\psi_{d,t,p}\right)}{\sum_{(t',p')\in C_d}\exp\left(\psi_{d,t',p'}\right)} \tag{15}$$

Here, $P_{d,t,p}$ represent the normalized probability of kalendolipid E acting on pathway p via target t. C_d represents all candidate target-pathway combinations of kalendolide E. The function of this formula is to compress the scattered relationship scores into directly comparable probability distributions, so that the priorities of different mechanism chains can be judged on the same scale.

Fig. 4 illustrates the overall structure of the relationship prediction model in this section. In the graph, starting from heterogeneous node embedding, a complete inference path of action chain is formed through edge weight updating, multi-step propagation, ternary relationship scoring, phenotype reversal fusion and probability output. Each layer in the diagram has a clear function and is not a side-by-side stacked submodule, but a continuous chain of computations around the resolution of the carenoglycoside E mechanism.

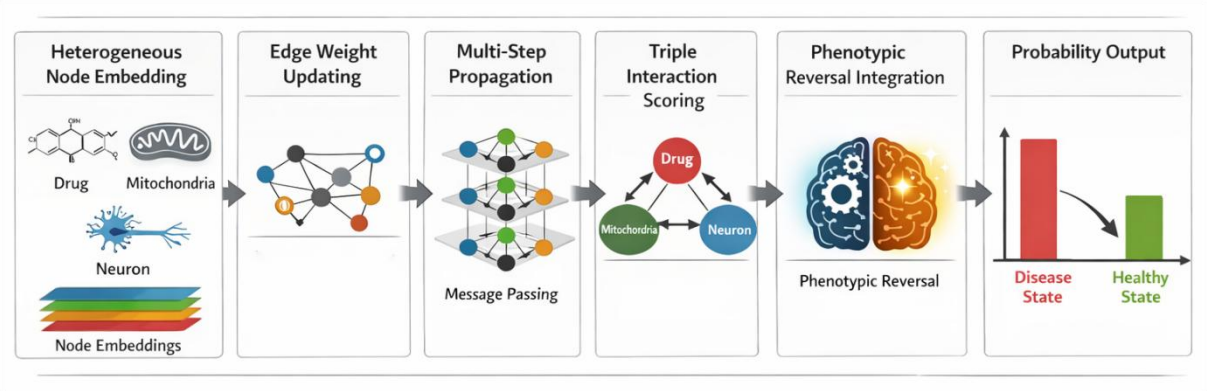

Figure 4: Structural diagram of carenpolyside E interaction prediction model for molecular mechanism analysis

After modeling in this section, the action of carenoglycoside E no longer stays at the planar comparison level of several independent candidate targets, but is organized into a continuous chain of action with structural propagation, directional constraints, and phenotypic correspondences. The model output can simultaneously give the core targets, key pathways and high-confidence relationship combinations of possible drug effects, and show the priority of the main pathway of the mechanism through the ranking results.

4 Verification of the molecular mechanism of kalendolide E regulating mitochondrial function to improve Parkinson's disease

4.1 Experimental design and model parameter setting

In order to verify the effectiveness of the molecular mechanism model of kalendolide E regulating mitochondrial function to improve Parkinson's disease, a unified experimental framework was constructed. The experimental data consists of transcriptome expression matrix, mitochondrial function annotation, protein interaction, drug docking response and Parkinson's disease phenotype label, which contains 1248 case and control samples, 312 mitochondrial related candidate molecules, 8640 high confidence interaction edges and 42 regulatory pathways. All samples were divided into training set, validation set and test set according to 7:1:2, and the consistency of disease status, molecular category and pathway distribution was maintained under stratified sampling condition. In the preprocessing stage, missing value repair, batch offset correction, extreme value truncation, vector normalization and semantic coding mapping are completed, so that the structural differences and functional boundaries can still be preserved after heterogeneous inputs enter the same computing space.

The experimental platform uses Ubuntu 22.04 operating system, Intel Xeon Gold 6330 processor, 128 GB memory and NVIDIA RTX 4090 graphics card, and the model is implemented by Python 3.11, PyTorch 2.2 and PyG graph learning library. AdamW optimizer was used in the training phase with the initial learning rate set to 0.0003, the weight decay coefficient set to 0.0001, the batch size set to 32, the maximum number of training rounds set to 180, and the number of early stopping rounds set to 20. The node embedding dimension is set to 128, the number of graph propagation layers is set to 3, the number of relation attention heads is set to 4, and Dropout is set to 0.15. The parameter search adopts a segmented grid strategy driven by the validation set, and the regularization term in the pattern recognition

weight, the pathway association weight and the relation ranking loss are calibrated preferentially to ensure that the convergence rhythm between different sub-modules is consistent.

To facilitate the presentation of the experimental configuration, the key environment and parameter Settings are shown in Table 4.

Table 4: Experimental environment and core parameters

Item	Setting
Data scale	1,248 samples, 312 candidate molecules, 8,640 interaction edges, and 42 pathways
Data split	Training, validation, and test sets were divided at a ratio of 7:1:2
Hardware environment	Ubuntu 22.04, Xeon Gold 6330, RTX 4090, and 128 GB memory
Software environment	Python 3.11, PyTorch 2.2, and PyG
Training parameters	AdamW, learning rate of 0.0003, weight decay of 0.0001, batch size of 32, and a maximum of 180 epochs
Model parameters	Embedding dimension of 128, 3 graph propagation layers, 4 attention heads, and a dropout rate of 0.15

The Settings in Table 4 are not simply listed, but are determined by three parts: molecular pattern recognition, target-pathway feature extraction and interaction relationship prediction. In the pattern recognition module, the fusion coefficients of expression layer, function layer and structure layer were set to 0.40, 0.35 and 0.25, respectively, to ensure that the mitochondrial localization information would not be obscured by high fluctuating expression values. The five types of weight validation sets in the association feature extraction stage are fixed to 0.22, 0.21, 0.19, 0.18 and 0.20 after comparison. The historical state retention coefficient in the relationship prediction module is set to 0.30, which can suppress over-smoothing and maintain the stability of the main path propagation. The three groups of comparison models adopt the same data division and training rounds synchronously, and only replace the core mechanism unit, so as to ensure that the results have a unified benchmark and interpretability. In this section, the experimental framework, operating environment and key parameters are set, and the experimental process has a stable basis for reproducibility.

4.2 Analysis of the molecular mechanism of kalendolide E regulating mitochondrial function to improve Parkinson's disease

After setting the experimental environment and parameters, this paper further analyzed the molecular mechanism of kalendolide E regulating mitochondrial function to improve Parkinson's disease. In order to make the evaluation results reflect the relationship identification ability, mechanism chain ranking ability and phenotype interpretation ability at the same time, we verify the model from four levels: overall performance, candidate main path hitting, repeated sampling stability and module contribution. We also compare the proposed model with Rule-Score, GraphSAGE-Path and HeteroGAT.

In order to visually present the overall differences of different models in multiple indicators, Fig. 5 uses radar charts to present five indicators: AUC, F1, Hit@10, NDCG@10 and Path-Consistency. In the figure, the corresponding values of the proposed model are 0.948, 0.921, 0.870, 0.889 and 0.903 respectively. HeteroGAT were 0.918, 0.887, 0.821, 0.836 and 0.861, respectively. GraphSAGE-Path is 0.901, 0.865, 0.793, 0.804 and 0.836; The Rule-Score is 0.856, 0.812, 0.731, 0.748, and 0.781. It can be seen that the proposed model is in the outermost

layer on the five indicators, indicating that the model is not only stronger in relation differentiation, but also maintains synchronous promotion in front ranking and path consistency.

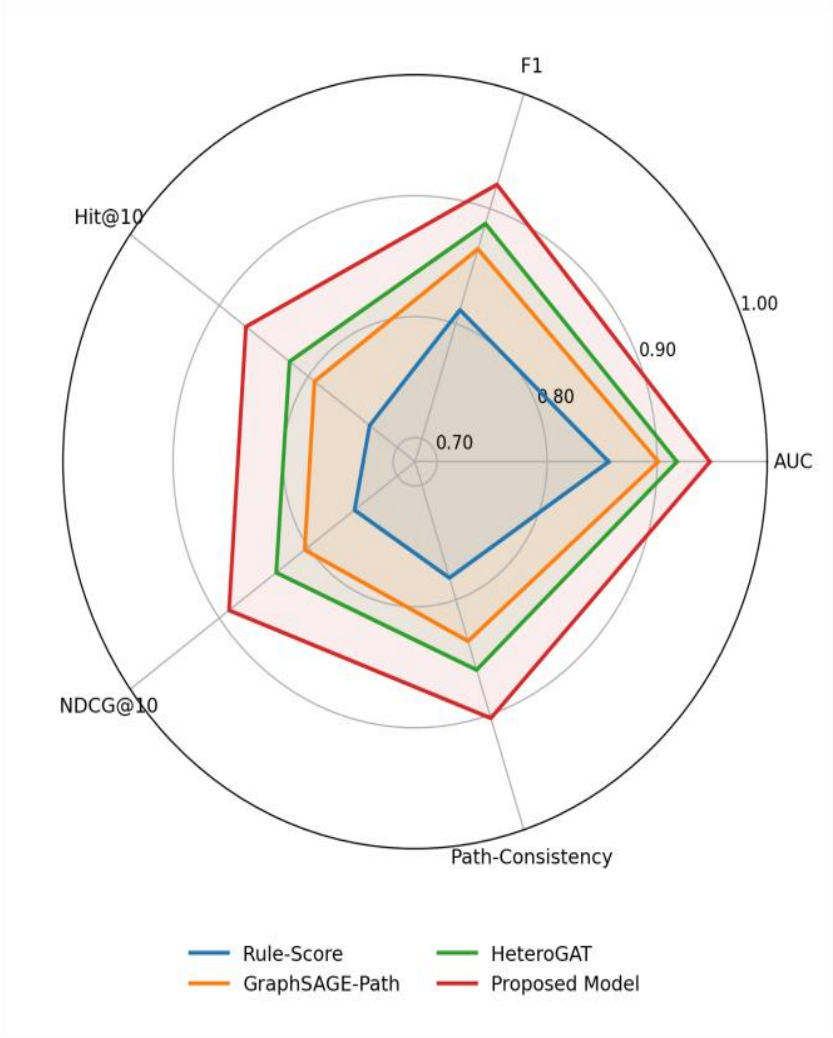

Figure 5: Comprehensive comparison radar chart of different models on mechanism chain ranking metrics

Table 5 lists the core evaluation results of the four models on the test set. It can be seen that the proposed model reaches 0.948, 0.921, 0.934, 0.909 and 0.850 on AUC, F1, Precision, Recall and Hit@20, respectively. It is 0.030, 0.034, 0.029, 0.038 and 0.037 higher than the sub-optimal model HeteroGAT. Seventeen of the top 20 candidate mechanism chains are consistent with the validation database and literature evidence, which indicates that the model not only improves the numerical index, but also pushes the more mechanism meaningful action chains to the top of the ranking.

Table 5: Core evaluation results of different models on the test set

Model	AUC	F1	Precision	Recall	Hit@20
Rule-Score	0.856	0.812	0.824	0.799	0.713
GraphSAGE-Path	0.901	0.865	0.879	0.852	0.781
HeteroGAT	0.918	0.887	0.905	0.871	0.813
Proposed Model	0.948	0.921	0.934	0.909	0.850

Comparing means alone is not enough to say whether the high-scoring relationship is stably distributed, so this paper continues to compare the relationship score distributions of different models. As shown in Fig. 6, the median of the proposed model is 0.824, the upper quartile is 0.891, and the lower quartile is 0.768. The overall distribution is centralized and the outliers are few. The median of HeteroGAT is 0.771, GraphSAGE-Path is 0.736, and Rule-Score is 0.694. This result shows that the performance improvement of the proposed model is not supported by individual samples, but forms an overall improvement on most candidate relations, and the internal stability of the model output is stronger.

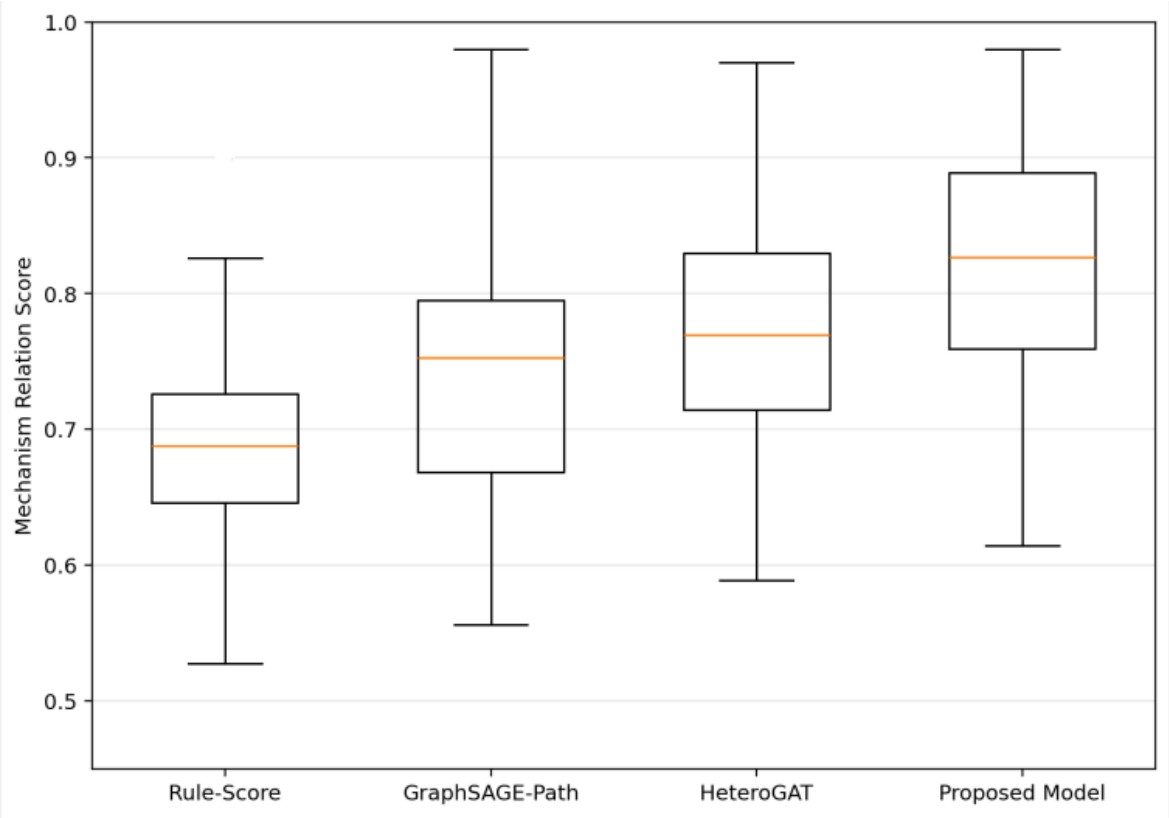

Figure 6: Boxplots of the distribution of score for different model mechanism relationships

To further observe the matching between kalendolin E and the mitochondrial core link, Fig. 7 uses heat maps to show the hit intensities of Top-12 high-confidence targets in six critical pathways. The results showed that AMPK-SIRT3, OPA1-mediated fusion, complex I homeostasis, ROS scavenging and membrane potential maintenance pathways showed continuous high responses. The association scores of SIRT3, OPA1, NDUFS2, PRDX3 and TFAM were 0.913, 0.901, 0.887, 0.874 and 0.862, respectively. The scores of non-core inflammatory bypass were mostly concentrated between 0.41 and 0.56. This phenomenon indicates that the output of the proposed model does not diffuse into loose extensive connections, but mainly compresses in the units related to mitochondrial homeostasis maintenance, and the path concentration is high.

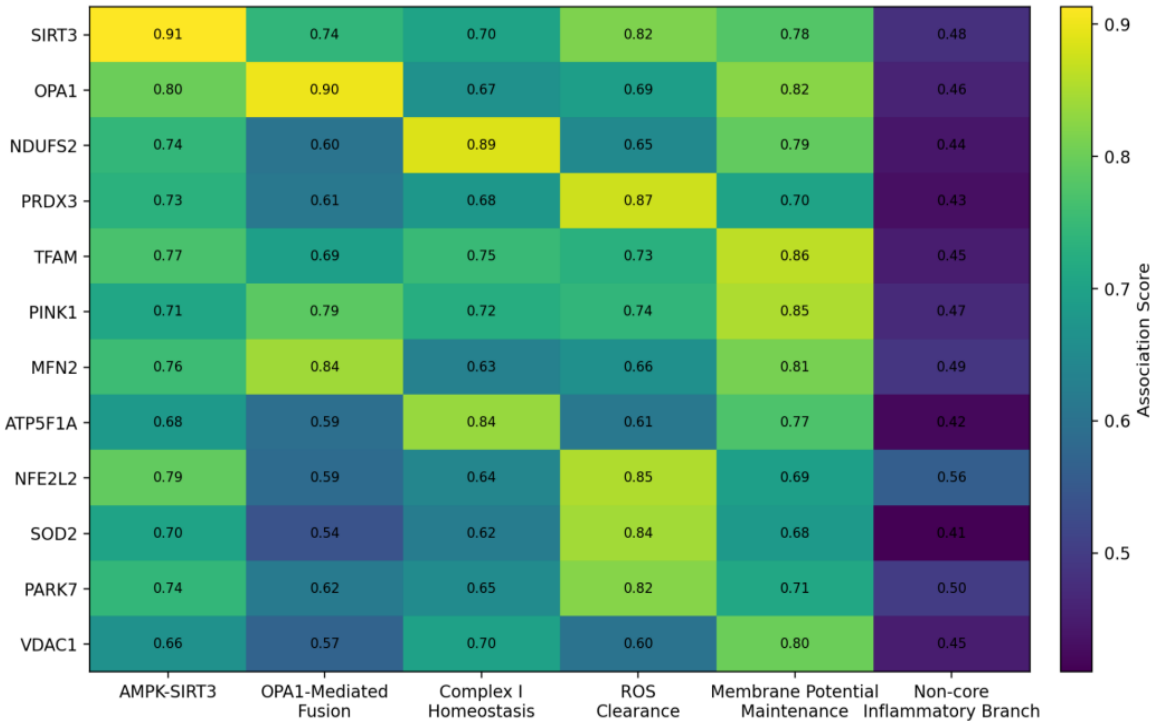

Figure 7: Hit heatmaps of Top-12 high-confidence targets versus key mitochondrial pathways

In addition to the pathway thermal distribution, it is also necessary to determine whether this centralized output can be stable under repeated sampling. To this end, Table 6 presents the ten-fold cross-validation results. The average AUC, AUC standard deviation, average F1, F1 standard deviation, average Hit@20 and Hit@20 standard deviation are retained in the table to measure the mean level and the fluctuation amplitude simultaneously. The average AUC of the proposed model is 0.941, and the standard deviation is 0.006. The average F1 is 0.914, and the standard deviation is 0.008. The average Hit@20 is 0.842 and the standard deviation is 0.010. Compared with the Rule-Score, the standard deviations of the three terms of HeteroGAT are 0.011, 0.014 and 0.018, and the standard deviations of GraphSAGE-Path are 0.013, 0.017 and 0.021, respectively. The smaller fluctuation indicates that the proposed model is not sensitive to the change of training set partition and noise disturbance, and the output results have better statistical stability.

Table 6: Results of ten-fold cross-validation statistics

Model	Mean AUC	AUC Std. Dev.	Mean F1	F1 Std. Dev.	Mean Hit@20	Hit@20 Std. Dev.
Rule-Score	0.847	0.018	0.804	0.021	0.704	0.026
GraphSAGE-Path	0.893	0.013	0.857	0.017	0.774	0.021
HeteroGAT	0.912	0.011	0.881	0.014	0.806	0.018
Proposed Model	0.941	0.006	0.914	0.008	0.842	0.010

To show the mechanistic main paths output by the model, Fig. 8 compares the combined probabilities of the top ten high-confidence action chains using a scatter plot. Path 1 "kalendolide E-SIRT3-AMPK-SIRT3 signals-improved survival of dopaminergic neurons" was

0.931, path 2 was 0.918, path 3 was 0.903, path 4 was 0.891, path 5 was 0.883, and path 3 was 0.903. The other five paths are 0.871, 0.859, 0.847, 0.829, and 0.812. The overall interval ranged from 0.812 to 0.931, and the first five maximum differences were only 0.048, indicating that the internal consistency of the high confidence mechanism chain was strong, and the ranking results were stably concentrated on the pathways related to mitochondrial homeostasis regulation, oxidative stress relief and neuronal survival maintenance.

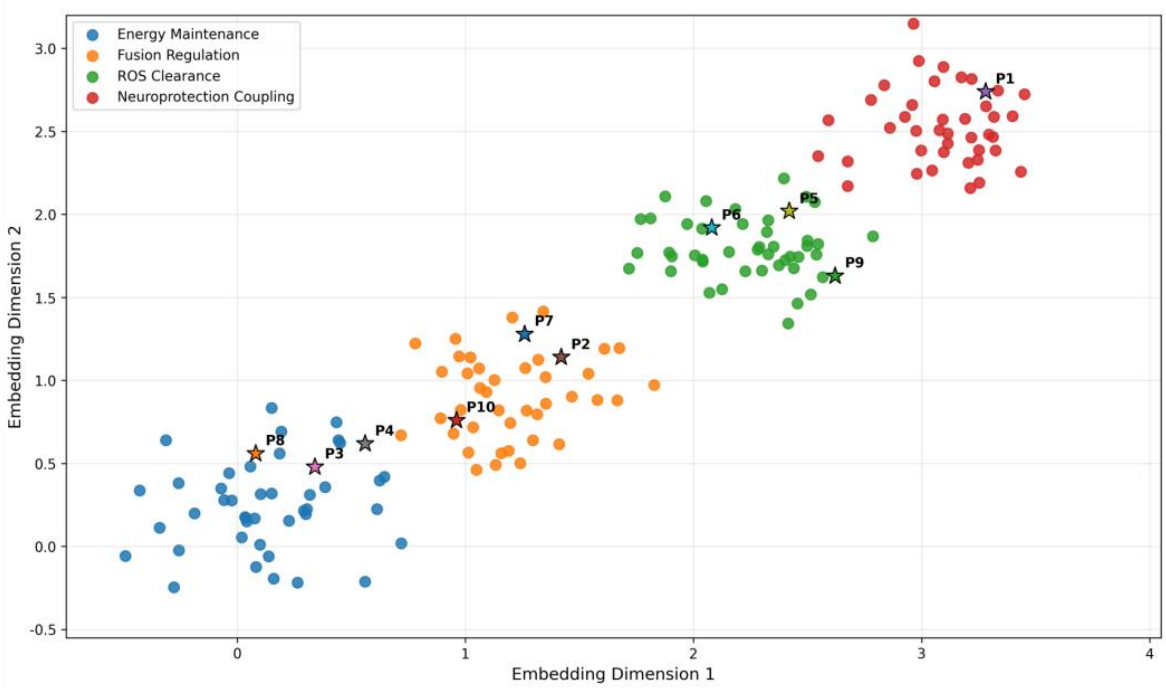

Figure 8: Scatter plot of integrated probabilities of primary paths for the top ten high-confidence mechanisms

After the overall performance, distribution status and main path output analysis, this paper continues to investigate the actual contribution of different modules through ablation experiments. Table 7 shows that the AUC, F1 and Hit@20 of the full model are 0.948, 0.921 and 0.850, respectively. After removing the molecular pattern recognition module, the number decreased to 0.917, 0.883 and 0.801. After removing the pathway association feature extraction, it is reduced to 0.910, 0.876 and 0.792. After removing the phenotypic reversal constraint, the values decreased to 0.923, 0.891 and 0.809. It decreases to 0.928, 0.896 and 0.817 after removing the relation ranking loss. It can be seen that molecular pattern recognition and pathway association extraction have the most obvious impact on the overall performance of the model, indicating that disease background compression and drug-pathway alignment are the two most critical types of supporting information in the ranking of mechanism chains.

Table 7: Comparison of the results of ablation experiments

Model Configuration	AUC	F1	Hit@20
Full Model	0.948	0.921	0.850
Without Molecular Pattern Recognition Module	0.917	0.883	0.801
Without Pathway Association Feature Extraction	0.910	0.876	0.792
Without Phenotype Reversal Constraint	0.923	0.891	0.809
Without Relation Ranking Loss	0.928	0.896	0.817

Synthesizing the results of this section, it can be seen that the proposed model shows consistent advantages in five aspects: overall performance, score distribution, main path concentration, repeated sampling stability and module synergy. More importantly, this advantage does not stop at the general classification performance level, but is specifically reflected in the compression of the high-confidence relationship between kalendolipid E and the core link of mitochondrial function. In other words, the model can not only identify which targets the drug may act on, but also organize these targets into a mechanism chain with directional and phenotypic correspondence, so that the computational analysis of the molecular mechanism of Parkinson's disease has higher structural interpretation strength and results credibility.

5 Discussion

The results of this paper show that the constructed mechanism analysis model does not rely on a single high-scoring target to determine the main pathway, but forms a more stable expression of drug action chain under the joint action of molecular pattern recognition, pathway association extraction and relationship propagation constraints. Compared with Rule-Score, graph structure propagation preserves the hierarchical connections between drugs, targets, pathways and phenotypes, and avoids excessive compression of kalendolide E action information in the multi-hop mapping process. Compared with GraphSAGE-Path and HeteroGAT, the proposed model writes both mitochondrial functional status and phenotypic reversal signals into the relationship score, so that high-confidence pathways not only show connectivity accessibility, but also show consistent regulatory direction. It can be seen from the first ten main pathways that SIRT3, OPA1, NDUFS2, TFAM and PINK1 do not appear in isolation, but form a relatively concentrated action cluster around energy maintenance, fusion regulation, oxidative stress relief and neuronal survival improvement. The results of 10-fold cross validation and ablation experiments are consistent with each other, indicating that the molecular pattern layer and pathway feature layer are not auxiliary structures, but key parts to support the ranking accuracy and the strength of mechanism explanation. The small difference between the front paths and the controlled overall fluctuation also indicate that the model output is not concentrated by chance, but is the result of building on stable parameter configurations and consistent functional constraints. This processing method extends from heterogeneous data fusion to mechanism chain inference, which enables the research of Parkinson's disease drug mechanism to have a clearer structural expression ability.

6 Conclusions

Focusing on the molecular mechanism of kalendolide E regulating mitochondrial function to improve Parkinson's disease, a computational framework consisting of molecular pattern recognition, pathway association feature extraction and interaction prediction was constructed. The results show that the framework can stably identify the drug-target-pathpathy-phenotype main path in heterogeneous networks, and compress key nodes such as SIRT3, OPA1, NDUFS2, TFAM and PINK1 into a unified mechanism chain, thereby enhancing the continuity and interpretability of mechanism analysis. In terms of AUC, F1, Hit@20 and cross-validation stability, the proposed model is better than the comparison methods, indicating that the collaborative design of relation ranking, phenotype constraint and graph propagation has high effectiveness. The limitations of this paper are mainly reflected in three aspects: the sample sources are still mainly public molecular data and computational annotations, and the

proportion of cross-platform experimental data is low. The intensity of drug action depends on static feature fusion, which has not been included in the time series response changes. The phenotypic layer verification is still dominated by computational evidence, and the depth of the closed loop of biological experiments is insufficient. Subsequent studies can continue to expand multi-cohort samples, introduce single cell time series trajectory and causality diagram modeling, combine cell and animal experiments to enhance the verification strength of mechanism chain, and further compress the scale of model parameters to construct a lightweight inference version suitable for drug screening scenarios. On this basis, similar natural active ingredients can also be included in the unified inference framework to test the transfer adaptation ability of the model in similar mechanism types, and improve its promotion value in the informatics research of neurodegenerative diseases.

Funding

Study on the Mechanism of Calenduloside E in Improving Parkinson's Disease by Inhibiting Mitochondrial Dysfunction-Induced Pyroptosis Signals
Project Number: 2025-3-085

References

[1] D’Sa K, Evans J R, Virdi G S, et al. Prediction of mechanistic subtypes of Parkinson’s using patient-derived stem cell models[J]. Nature Machine Intelligence, 2023, 5(8): 933-946.

[2] Payne T, Burgess T, Bradley S, et al. Multimodal assessment of mitochondrial function in Parkinson's disease[J]. Brain, 2024, 147(1): 267-280.

[3] Reddy A, Reddy R P, Roghani A K, et al. Artificial intelligence in Parkinson's disease: Early detection and diagnostic advancements[J]. Ageing research reviews, 2024, 99: 102410.

[4] Gupta R, Kumari S, Senapati A, et al. New era of artificial intelligence and machine learning-based detection, diagnosis, and therapeutics in Parkinson’s disease[J]. Ageing research reviews, 2023, 90: 102013.

[5] Tabashum T, Snyder R C, O'Brien M K, et al. Machine learning models for Parkinson disease: systematic review[J]. JMIR medical informatics, 2024, 12(1): e50117.

[6] Altham C, Zhang H, Pereira E. Machine learning for the detection and diagnosis of cognitive impairment in Parkinson’s Disease: A systematic review[J]. Plos one, 2024, 19(5): e0303644.

[7] Hähnel T, Raschka T, Sapienza S, et al. Progression subtypes in Parkinson’s disease identified by a data-driven multi cohort analysis[J]. npj Parkinson's Disease, 2024, 10(1): 95.

[8] Hossain M A, Amenta F. Machine learning-based classification of Parkinson’s disease patients using speech biomarkers[J]. Journal of Parkinson’s Disease, 2024, 14(1): 95-109.

[9] Ding C W, Ren Y K, Wang C S, et al. Prediction of Parkinson's disease by transcranial sonography-based deep learning[J]. Neurological Sciences, 2024, 45(6): 2641-2650.

[10] Yang H, Chen Y, Zuo Y, et al. MINDG: a drug–target interaction prediction method based on an integrated learning algorithm[J]. Bioinformatics, 2024, 40(4): btae147.

[11] Jiang H, Du Y, Lu Z, et al. Radiomics incorporating deep features for predicting Parkinson's disease in 123I-Ioflupane SPECT[J]. EJNMMI physics, 2024, 11(1): 60.

[12] de Lope E G, Loo R T J, Rauschenberger A, et al. Comprehensive blood metabolomics profiling of Parkinson's disease reveals coordinated alterations in xanthine metabolism[J]. npj Parkinson's Disease, 2024, 10(1): 68.

[13] Hällqvist J, Bartl M, Dakna M, et al. Plasma proteomics identify biomarkers predicting Parkinson's disease up to 7 years before symptom onset[J]. Nature communications, 2024, 15(1): 4759.

[14] Wu J, Wu W, Jiang P, et al. Identification of SV2C and DENR as key biomarkers for Parkinson's disease based on bioinformatics, machine learning, and experimental verification[J]. Journal of Molecular Neuroscience, 2024, 74(1): 6.

[15] Martirosyan A, Ansari R, Pestana F, et al. Unravelling cell type-specific responses to Parkinson's Disease at single cell resolution[J]. Molecular neurodegeneration, 2024, 19(1): 1-24.

[16] Smajić S, Prada-Medina C A, Landoulsi Z, et al. Single-cell sequencing of human midbrain reveals glial activation and a Parkinson-specific neuronal state[J]. Brain, 2022, 145(3): 964-978.

[17] Kamath T, Abdulraouf A, Burris S J, et al. Single-cell genomic profiling of human dopamine neurons identifies a population that selectively degenerates in Parkinson's disease[J]. Nature neuroscience, 2022, 25(5): 588-595.

[18] Kim J B, Kim S J, So M, et al. Artificial intelligence-driven drug repositioning uncovers efavirenz as a modulator of α-synuclein propagation: implications in Parkinson's disease[J]. Biomedicine & Pharmacotherapy, 2024, 174: 116442.

[19] Zhang Z, Chen L, Zhong F, et al. Graph neural network approaches for drug-target interactions[J]. Current Opinion in Structural Biology, 2022, 73: 102327.

[20] Long Y, Wu M, Liu Y, et al. Pre-training graph neural networks for link prediction in biomedical networks[J]. Bioinformatics, 2022, 38(8): 2254-2262.